AFRL-RX-WP-TP-2008-4349

IMPLEMENTATION OF EXACT GRAIN-BOUNDARY GEOMETRY INTO A 3D MONTE-CARLO (POTTS) MODEL FOR MICROSTRUCTURE EVOLUTION (PREPRINT)

O.M. Ivasishin, S.V. Shevchenko, and S.L. Semiatin

Metals Branch
Metals, Ceramics, and NDE Division

JULY 2008

AIR FORCE RESEARCH LABORATORY
MATERIALS AND MANUFACTURING DIRECTORATE
WRIGHT-PATTERSON AIR FORCE BASE, OH 45433-7750
AIR FORCE MATERIEL COMMAND
UNITED STATES AIR FORCE

REPORT DOCUMENTATION PAGE

Form Approved
OMB No. 0704-0188

1. REPORT DATE *(DD-MM-YY)*	2. REPORT TYPE	3. DATES COVERED *(From - To)*
July 2008	Journal Article Preprint	

4. TITLE AND SUBTITLE

IMPLEMENTATION OF EXACT GRAIN-BOUNDARY GEOMETRY INTO A 3D MONTE-CARLO (POTTS) MODEL FOR MICROSTRUCTURE EVOLUTION (PREPRINT)

5a. CONTRACT NUMBER
In-house

5b. GRANT NUMBER

5c. PROGRAM ELEMENT NUMBER
62102F

6. AUTHOR(S)

O.M. Ivasishin and S.V. Shevchenko (Institute for Metal Physics)
S.L. Semiatin (AFRL/RXLMP)

5d. PROJECT NUMBER
4347

5e. TASK NUMBER
RG

5f. WORK UNIT NUMBER
M02R2000

7. PERFORMING ORGANIZATION NAME(S) AND ADDRESS(ES)

Institute for Metal Physics

Metals Branch (AFRL/RXLMP)
Metals, Ceramics, and NDE Division
Materials and Manufacturing Directorate
Wright-Patterson Air Force Base, OH 45433-7750
Air Force Materiel Command, United States Air Force

8. PERFORMING ORGANIZATION REPORT NUMBER
AFRL-RX-WP-TP-2008-4349

9. SPONSORING/MONITORING AGENCY NAME(S) AND ADDRESS(ES)

Air Force Research Laboratory
Materials and Manufacturing Directorate
Wright-Patterson Air Force Base, OH 45433-7750
Air Force Materiel Command
United States Air Force

10. SPONSORING/MONITORING AGENCY ACRONYM(S)
AFRL/RXLMP

11. SPONSORING/MONITORING AGENCY REPORT NUMBER(S)
AFRL-RX-WP-TP-2008-4349

12. DISTRIBUTION/AVAILABILITY STATEMENT
Approved for public release; distribution unlimited.

13. SUPPLEMENTARY NOTES
Journal article submitted to the *Acta Materialia*. PAO Case Number: WPAFB 08-4044; Clearance Date: 10 Jul 2008. The U.S. Government is joint author of this work and has the right to use, modify, reproduce, release, perform, display, or disclose the work.

14. ABSTRACT

A three-dimensional Monte-Carlo (Potts) model was modified to incorporate the effect of grain-boundary inclination on boundary mobility. For this purpose, a straightforward geometric construction was developed to determine the local orientation of the grain-boundary plane. The combined effects of grain-boundary mobility were incorporated into the Monte-Carlo code using the definition of the tilt-twist component (TTC). The modified code was validated by simulating grain growth in microstructures comprising equiaxed or elongated grains as well as the static recrystallization of a microstructure of deformed (elongated) grains.

15. SUBJECT TERMS
Recrystallization, Grain growth, Grain boundary inclination, Monte Carlo technique

16. SECURITY CLASSIFICATION OF:			17. LIMITATION OF ABSTRACT:	18. NUMBER OF PAGES	19a. NAME OF RESPONSIBLE PERSON (Monitor)
a. REPORT	b. ABSTRACT	c. THIS PAGE			Sheldon L. Semiatin
Unclassified	Unclassified	Unclassified	SAR	24	19b. TELEPHONE NUMBER *(Include Area Code)* N/A

Implementation of Exact Grain-Boundary Geometry into a 3D Monte-Carlo (Potts) Model for Microstructure Evolution

O.M. Ivasishin *, S.V. Shevchenko*, and S.L. Semiatin**

*Institute for Metal Physics, 36 Vernadsky Str., 03142 Kiev, Ukraine

**Air Force Research Laboratory, AFRL/RXLM,
Wright-Patterson Air Force Base, OH 45433-7817 USA

Abstract

A three-dimensional Monte-Carlo (Potts) model was modified to incorporate the effect of grain-boundary inclination on boundary mobility. For this purpose, a straightforward geometric construction was developed to determine the local orientation of the grain-boundary plane. The combined effects of grain-boundary plane and misorientation on the effective grain-boundary mobility were incorporated into the Monte-Carlo code using the definition of the tilt-twist component (TTC). The modified code was validated by simulating grain growth in microstructures comprising equiaxed or elongated grains as well as the static recrystallization of a microstructure of deformed (elongated) grains.

Key words: Recrystallization, Grain growth; Grain boundary inclination; Monte Carlo technique

1. Introduction

There is a growing demand for mesoscale models describing the evolution of microstructure and texture during the thermomechanical processing (TMP) of materials. In particular, grain growth in polycrystalline metals has been studied extensively using both analytical and computer-based models. Among the various numerical methods, the Monte-Carlo (MC) Potts method, developed originally for the two-dimensional case in the 1980s by Anderson et al. [1, 2], has found widespread use to quantify the temporal evolution of grain shape and size. During the last decade, a number of specific efforts have focused on the *three-dimensional* simulation of grain growth, including comparisons with observations of the actual kinetics of microstructure evolution [3-8].

Recently, refined models have been formulated to treat the simultaneous evolution of microstructure and texture during TMP [9, 10]. For example, anisotropic grain-boundary (GB) properties have been taken into account; in these cases, the driving force for the migration of a particular grain boundary depends on both its curvature and crystallographic features. In other work, relatively straightforward modification of the classic 3D MC Potts technique [1-6] has enabled simulations for modeling domains (MD) with dimensions as large as 250×250×250 points or model units (MU). In such cases, it is possible to preserve an adequate number of grains to obtain statistically significant textures and grain size/GB distributions. Due to the large variety of possible misorientations as well as orientations of the actual boundary planes, however, there is a huge number of GBs with different structures and thus properties. To simplify modeling procedures and save computational resources and time, therefore, it has frequently been

assumed in previous MC Potts models of microstructure evolution that GB energy and mobility depend on the misorientation between adjacent grains but not on the specific spatial orientation of the boundary plane.

The assumption that GB properties depend only on misorientation is certainly not true. According to recent experimental measurements and molecular-dynamics simulations, GB energy and mobility are sensitive to not only the GB misorientation (GBM), but also to the orientation of the GB plane relative to the crystal lattices of the adjacent grains, i.e., the grain-boundary inclination (GBI). According to Reference 11, for example, the mobility of Σ5 [010] tilt boundaries in pure nickel is very dependent on GBI; in this work, it was determined experimentally that the mobility varied by a factor of 2 to 4 with GBI. It was also found experimentally that the relative energy of selected high-angle, *non-special* GBs in NiAl vary over a wide range (0.47 to 1) depending on GBI [12]. An additional confounding factor in the description of GB properties for real polycrystalline materials is the fact that the GBI changes along curved GBs, unlike GBM, and thus must be quantified locally.

Another important feature of real materials is the fact that not all possible GBIs are present in equal quantities [13, 14]. Hence, the probability distribution for the normal to the GB plane (so-called GB-plane textures) can be presented as pole figures. For Cu, Ni, and Ti-6Al-4V [13, 14], there can be very strong GB-plane textures which are only partially related to twinning and which persist even after long-duration, low-temperature annealing.

To improve the fidelity of 3D MC models for microstructure evolution, the local GBI must be introduced. This certainly makes the modeling routine more complex relative to earlier approaches [9] in which the GBM is presented in a simple scalar form. First, an exact matrix form which can be reduced to a three-component vector is needed to accommodate the introduction of the local GB geometry. Second, if successful, such model enhancements would require a database on GB properties for all possible combinations of GBM and GBI. Although such information is not currently available in a systematic form, substantial experimental and theoretical efforts are in progress. They have already provided experimental data which are sufficiently accurate to investigate model validity and performance.

The effect of GBI on boundary migration is easily introduced into analytical models of grain growth which utilize GB surfaces and triple-junction lines as analytical functions [15, 16]. Similar formulations in numerical approaches are usually restricted to 2D cases or the 3D modeling of the evolution of grain topology. However, such methods are usually not suitable for the numerical modeling of texture evolution. For instance, in 3D MC modeling, the analytical approach to GB tracking is not used because the GBI changes continuously as the GB migrates. Hence, information obtained during previous MC steps cannot be used for subsequent ones. Therefore, it is not worthwhile to fit an analytical function to the GB geometry because one needs to repeat this time-consuming procedure after each elementary MC event.

The objective of the present work was to incorporate the *locally-estimated* GBI into a 3D MC Potts model of grain growth. GBI effects were examined recently using a 2D cellular-automaton (CA) model for microstructure evolution [17], but cannot be extended for the 3D case. The present paper presents an initial attempt to meet this need for the 3D case. The discussion below deals with (1) the calculation of the local GBI and

an efficient procedure of its estimation within a 3D MC Potts code, (2) an optimization procedure for estimating GBI and an analysis of associated errors, and (3) model-validation examples to establish how the inclusion of GBI affects predictions of grain-growth and recrystallization kinetics.

2. Approach for incorporating GBI into an MC Potts simulation

The refinements presented in this section were incorporated into a previously developed 3D MC Potts model [9] which has been used to simulate simultaneous grain growth and texture evolution in polycrystalline materials. The model and associated software have also been used to describe abnormal grain growth [18]. Thus, only a brief description of the basic approach is given here.

The model domain is formed by a 3D cubic array of MUs, each of which represents a point in a cubic lattice. Each MU is assigned an integer corresponding to its specific orientation in Euler space. As in previous work utilizing the MC approach [9, 17], the model domain does not contain grain boundaries *per se.* Rather, grain-boundary positions are associated with the space between two sites having dissimilar orientations. The size of each grain is taken to be equal to the diameter of a sphere containing the same volume (i.e., number of MUs).

During one Monte-Carlo Step (MCS), the number of elementary flip-simulation trials is equal to the number of sites in the model domain. Hence, the local velocity of a grain boundary is measured in terms of MU/MCS, and has the maximum possible value of 1 MU/MCS. In each elementary flip-simulation trial, the sampling neighborhood, or control volume, is characterized by a search radius equal to 2 MU. Thus, 124 nearest MUs are taken into account in the cubic 3D array.

As mentioned above, it appears that only one prior attempt [18] has been made to introduce a dependence of GB properties on GBI in a mesoscale numerical model. In this former 2D CA work, GB displacements were allowed to occur as *fractional* increments of the size of an individual cell, thus emulating continuous, not discrete, tracking of the boundary location with time. The modified approach in Reference 18 yielded a better description of grain-growth phenomena, but required substantial additional data-storage resources. A correlation between the GB normal direction and the incremental (scalar) cell displacement was noted, albeit for the 2D case of interest in which merely one angle determines the normal. Such an approach can not be extended to 3D because two independent angles for the GB normal direction can not be estimated from scalar displacement increments. Hence, an alternate procedure is required for 3D mesoscale simulations.

For the present 3D case, the GB was represented by the function $z = f(x,y)$. The local GBI at point $M_o(x, y, z)$ was quantified using planar linear approximations for the two orthogonal Cartesian cross-sections through it lying parallel to the *xz* and *yz* planes (Fig. 1). The partial derivatives $\partial f/\partial x$ and $\partial f/\partial y$ define a tangential line for each cross-section. The tangential *plane* for $z = f(x,y)$ was thus defined by these two tangents forming angles α and β with the reference coordinate axes (Fig.1). The normal to the tangential plane, which characterizes the GBI at point M_o, is then

$$\overline{m} = \left(\frac{\partial f}{\partial x}(M_o); \frac{\partial f}{\partial y}(M_o); -1\right), \qquad (1)$$

and the equation for the normal line (which includes the given MU) is given by :

$$\frac{x-x_o}{\frac{\partial f}{\partial x}(M_o)} = \frac{y-y_o}{\frac{\partial f}{\partial y}(M_o)} = \frac{z-z_o}{-1} \qquad (2)$$

A special algorithm was developed to determine the local GBI within the MC code. For each cross-section, the nearest 48 MUs at the location of interest were utilized (Fig. 2a). Although two Cartesian cross-sections are sufficient for the linear approximations defining the GBI, there are instances for which the number of MUs within one of them is not enough (Fig 2b). In such cases, *three* Cartesian cross-sections were used to guarantee that at least two were suitable for the linear approximation.

The implementation of the exact GB description into the 3D MC code also required usage of an exact GB misorientation (GBM), instead of the usual scalar approximation. Previously, the single parameter ε consisting of the lattice misorientation between neighboring grains was used to define the relative grain-boundary energy and mobility [3-10]:

$$\varepsilon = \arccos\left(\frac{m_{11}+m_{22}+m_{33}-1}{2}\right). \qquad (3)$$

The use of the scalar parameter ε overlooks important GB features, such as the tilt-twist character. Hence, the MC routine was modified to incorporate the exact matrix misorientation **S** between grains having orientations g_1 and g_2 :

$$\mathbf{S} = \mathbf{S}_{g_1} \times \mathbf{S}_{g_2}^{-1} = \begin{pmatrix} m_{11} & m_{12} & m_{13} \\ m_{21} & m_{22} & m_{23} \\ m_{31} & m_{32} & m_{33} \end{pmatrix}, \qquad (4)$$

In Equation (4), the rotation matrices $\mathbf{S}_{g_1}$ and $\mathbf{S}_{g_2}$ correspond to orientations g_1 and g_2 of the neighboring grains. From a computation standpoint, an evaluation of the matrix form of the misorientation would require a prohibitive amount of time if done for each MC trial, even if such calculations utilized an efficient scheme such as that based on quaternions [19]. Therefore, a database of **S** as a discrete function of g_1 and g_2 was pre-calculated and loaded into the computer memory prior to executing model calculations. Thus, only a simple search operation was performed for each MC trial.

3. Errors associated with GBI calculations

The errors associated with the above procedure for calculating the GBI were assessed using a series of isolated, perfectly spherical grains of different initial radii R. Such trials ensured that all possible GBIs and curvatures would be evaluated for situations in which the exact GB tangent plane could be determined analytically.

Fig. 3a illustrates the specific geometry, indicating the cross-section of a typical spherical grain and its normal estimated using the procedure described in Section 2. The acceptable average error, i.e., the angular difference between the exact and estimated

normals, was taken to be 2 degrees, a value comparable to the typical Euler-angle step size used in the representation of orientations in MC modeling procedures. This specification is somewhat more conservative than the usual angular step (5 degrees) used for orientation-distribution function (ODF) analysis.

The GBI calculations for isolated grains of different sizes revealed errors which were acceptable for more than 99 pct. of the cases involving radii above 20 MU (Table 1). For small radii, the fraction of acceptable estimates dropped to 94 pct. For grain radii above 50 MU, the average GBI error remained essentially constant, i.e., the result did not improve with further increases in grain radius.

Figures 3b, c illustrate the origin of errors in estimating the GBI for large and small radii of curvature, respectively. The procedure cannot quantify the GBI for small grains/GB segments because the whole GB/grain segment is smaller than the area shown in Fig. 2a. For fine microstructures, it is thus necessary to use a 5×5 MU working area, which still gives acceptable results. Furthermore, the procedure cannot be used to estimate the GBI for GB segments close to triple junctions because the specific GB segments here are also smaller than the working area. Hence, if M_0 in an MC simulation is located close to a triple line or junction (Fig. 4a), it is impossible to derive the GBI due to the low resolution of the model grid. More specifically, Figure 4b illustrates the spatial limitations for the determination of the GBI determination. Because at least 4 MUs nearest to the GB point M_0 must be present within each Cartesian cross-section, the procedure will not work with GB radii less then 4 MUs. To overcome the challenge associated with triple lines/junctions (indicated in black in Fig. 4b), a procedure was introduced to exclude such areas from the GBI calculation. Figure 4c illustrates the fraction of the GB network as a function of average grain size for which the GBI can be estimated correctly.

4. Validation of the MC Potts model of grain growth using exact GB geometry

To account for both GBM and GBI in the present simulations of grain growth and recrystallization, the effective grain-boundary mobility M, which is a function of these two quantities and is normalized to a maximum value of unity, was introduced. There is no systematic database for M. Nevertheless, the functional dependence of M can be assumed to consist of a surface with lower mobilities for low-angle boundaries (e.g., References 18 and 20) and a maximum at values of the so-called tilt-twist component (TTC) of ~0.1-0.3, per available experimental measurements [12, 21]; the specific surface used in the present simulations is given in Fig. 5. Per reference 12, the TTC component is defined as the dot product of the unit vector parallel to the GB misorientation rotation axis and the local GB plane unit normal. The GB-misorientation rotation axis can be derived from the misorientation matrix M (Eq. 4), i.e.,

$$\{U,V,W\} = \{\frac{(m_{23}-m_{32})}{Z} \quad \frac{(m_{31}-m_{13})}{Z} \quad \frac{(m_{12}-m_{21})}{Z}\};$$
$$Z = \sqrt{(m_{23}-m_{32})^2+(m_{31}-m_{13})^2+(m_{12}-m_{21})^2} \qquad (5)$$

The value of the TTC varies from 0 for pure tilt GBs to 1 for pure twist GBs. The general case of 0 < TTC < 1 thus describes a mixed type of GB with the TTC representing the fraction of the twist component in the GB.

4.1. Initial test case

A relatively simple grain-growth example was used as an initial test of the MC model incorporating the description of GBI. To demonstrate the effect of GBI-dependent effective mobility on the evolution of grain structure, the problem consisting of the shrinkage of a spherical grain (initial R = 100 MU) was simulated; this problem is similar to that used in Reference 9 to validate the original 3D MC code. For this example, the misorientation between the matrix and grain was taken to be 35°. In the original simulation [9], in which the mobility depended only on the scalar misorientation, the grain remained essentially perfectly spherical until it disappeared. In present case, the GBI is well defined at every point on the grain boundary. Because the misorientation was constant, the effective mobility M = *f* (GBM, GBI) corresponded to the specific section indicated by the red line in Fig. 5. As expected, the variation of GBI resulted in the prediction of different GB migration rates for different local values of TTC (Fig. 6), resulting in distortion of the original spherical shape as the grain shrunk.

4.2. Grain growth modeling using the exact GB geometry

Three more detailed MC simulation cases (denoted A, B, C) were run to clarify the effect of GBI-dependent effective mobility on grain growth. For Case A**,** the GB effective mobility was assumed to be a function of GB misorientation only, while for Cases B and C the effective mobility dependence shown in Figure 5 was assumed. Two cases (A, B) were designed to elucidate the effect of grain-boundary mobility as function of GBI on grain-growth kinetics for an initial, nearly equiaxed microstructure (Figure 7a). This microstructure had 1000 grains within the 250^3 MU domain and hence an initial average grain size of 31 MU. For the nearly equiaxed grain shape the GBI distribution was relatively wide (Cases A and B). The volumes were not textured initially; hence, the effect of GBM on GB motion for Cases A and B was the same.

Case C was run to establish the specific influence of GBI on grain-growth kinetics via use of a microstructure with a non-equiaxed grain morphology (Figure 7c). In particular, the initial microstructure for Case C comprised grains with the same average grain size as for cases A and B, but having an aspect ratio of 1:3:3 (Figure 7c). In this instance, therefore, the initial GBI distribution was relatively narrow in comparison to that for the equiaxed microstructure. The initial grain-size distributions for the three cases are shown in Figures 7b, d.

As expected, the kinetics for Case A (Figure 8) mimicked so-called normal grain growth for which the average grain size is proportional to the square root of time. For Case B, the initial growth stage was slower than for Case A due to the lower effective GB mobility for boundaries whose inclination varied mostly around a pure tilt direction. After approximately 100 MCS, grain growth became faster for Case B due to the evolution of grain boundaries with higher effective mobility, but then slowed again. Further alternating periods of faster and slower grain growth could then be expected for longer times, a behavior similar to previous observations for strongly-textured materials [9].

For Case C, an initial increment of time was required for the first several smaller grains in the initial grain-size distribution (Fig. 7) to vanish. As a result, the initial rate of increase in the average grain size for this case was very small (Figure 8). In general, due to the specific GBI distribution, the grain-growth kinetics for a non-equiaxed microstructure were found to be much slower. Nevertheless, it was observed that the microstructure gradually transformed into an equiaxed one. After reaching an aspect ratio of 1:1:1 , the grain-growth kinetics for Case C were, as expected, similar to those for Cases A and B, although the delay at the beginning stage of the growth resulted in a smaller average grain size.

4.3. MC Simulation of recrystallization

MC simulations were also conducted to establish the effect of GBI distribution on the recrystallization kinetics of deformed textured materials. The initial, as-deformed microstructure had grains with an aspect ratio of 1:3:3 (Fig. 9), as in Case C, thus providing a narrow GBI distribution, and a sharp, single-component initial texture strong enough so that most grains were similarly oriented. The initial stored-energy distribution (Fig. 10) was assumed to be highest close to GBs and decrease toward the interior of the grains. Oriented, continuous nucleation of recrystallized grains was assumed. New grains were assumed to be misoriented 30 - 45 degrees to the deformed matrix, but the rotation axes were randomly selected. Furthermore, it was assumed that grain boundaries were preferred sites for nucleation of recrystallized grains. The nucleation rate within the unrecrystallized material was set as 10^{-4} nuclei per MU^3 per MCS. Recrystallization nuclei were assumed to be equiaxed with an average volume of 15 MU^3. The recrystallization front velocity was proportional to the local stored-energy density and the effective mobility. In Case D, the GB mobility was assumed to be a function of GB misorientation only, such that low-angle boundaries (LABs) were assumed to have low mobility relative to high-angle boundaries (HABs). For Case E, the mobility was a function of both misorientation and GBI using the dependence shown in Fig. 5.

Microstructural changes during recrystallization for Cases D and E after an equal number of MCS are illustrated in Fig. 11. For the assumed stored-energy distribution and nucleation conditions, the average GBI for the recrystallization front was approximately the same as for the as-deformed material (Fig. 11b). Because recrystallization kinetics depend on the effective mobility, it would be expected that they would be slower when the mobility-dependence on GBI is taken into account. In fact, the MC simulation results for Cases D and E did show a noticeable effect in terms of the recrystallization rate and the time to complete recrystallization (Fig. 12). Fig. 13 shows the microstructures for Cases D and E after the completion of recrystallization. The predicted average grain size for Case E was about two times as large that for Case D; i.e., 32 and 18 MUs, respectively.

5. Conclusions

A 3D Monte-Carlo (Potts) code was modified to quantify the effect of grain-boundary inclination (GBI) on mobility and thus on microstructure evolution during recrystallization and grain-growth processes. The following conclusions were drawn from this work:

1. The inclination of grain boundaries in MC simulations can be determined within 2 degrees by a relatively simple geometric construction except for very small

grains (< 20 MU radius) and near triple points/triple lines. In these cases, the fitting procedure should focus on a smaller neighborhood/number of MUs.

2. Using realistic data for mobility as a function of misorientation and the tilt/twist component (TTC), which incorporates the GBI, grain-growth kinetics can be readily predicted. MC simulations incorporating the exact grain-boundary character reveal periods of fast and slow grain growth, a behavior qualitatively similar to that previously found for texture-controlled grain growth.

3. MC simulations incorporating the effect of GBI on mobility reveal that static recrystallization kinetics can be noticeably retarded for realistic boundary properties and initial deformed grain shapes relative to simulations in which GBI is not taken into account.

Acknowledgements. The present work was supported by the Air Force Office of Scientific Research (AFOSR) and the AFOSR European Office of Aerospace Research and Development (AFOSR/EOARD) (W.S. Sanders and K.J. LaRochelle, Program Managers) within the framework of STCU Partner Project P-262.

References

1. Anderson MP, Srolovitz DJ, Grest GS, Sahni PS, Acta Metall 1984; **32**:783
2. Srolovitz DJ, Grest GS, Anderson MP, Rollett AD, Acta Metall 1988; **36**:2115
3. Miodownik MA, Godfrey AW, Holm EA, Hughes DA, Acta Mater 1999; **47**:2661
4. Raabe D, Acta Mater 2000; **48:**1617
5. Yang Z, Sista S, Elmer JW, Debroy, T., Acta Mater 2000; **48**:4813
6. Wakai F, Enomoto N, Ogawa H, Acta Mater 2000; **48**:1297
7. Xiaoyan S, Guoquan L, Nanju G, Scripta Mater 2000; **43**:355
8. Holm EA, Hassold GN, Miodownik MA, Acta Mater 2001; **49**:2981
9. Ivasishin OM, Shevchenko SV, Vasiliev NL, Semiatin SL, Acta Mater 2003; **51:**1019
10. Ivasishin OM, Shevchenko SV, Vasiliev NL, Semiatin SL, Mater Sci Eng A 2006; **433**:216
11. Zhang H, Mendelev MI, Srolovitz DJ, Scripta Mater 2005; **52**:1193
12. Amouyal Y, Rabkin E, Mishin Yu, Acta Mater 2005; **53**:3795
13. Randle V, Rohrer GS, Hu Y, Scripta Mater 2008; **58**:183
14. Randle V, Rohrer GS, Miller HM, Coleman M, Owen GT, Acta Mater 2008; **56**:in press
15. Chen JS, Kotta V, Lu H, Wang D, Moldovan D, Wolf D, Comput. Methods Appl. Mech. Eng 2004; **193**:1277
16. Slotemaker AK, de Bresser JHP, Tectonophysics 2006; **427 :**73
17. Raghavan S, Sahay SS, Mater Sci Eng A 2007; **445-446**:203
18. Ivasishin OM, Shevchenko SV, Semiatin SL, Scripta Mater 2004:**50**, 1241
19. Sutton AP, Balluffi RW, in: Interfaces in Crystalline Materials, Clarendon Press, Oxford, 1995.
20. Rollett AD, Holm E, in: McNelley T.R., ed. Proc. Of the 3rd Int. Conf. on Recrystallization and Related Phenomena, Monterey, USA, 1997, p. 31.

21. Gottstein G, Shvindlerman LS, in: Grain Boundary Migration in Metals., CRC Press LLC, 1999, p. 184.

Table 1. Error (angle between estimated and exact GB normal) as a function of GB radius of curvature (R) based on 200 measurements for randomly selected GB segments for each R

Radius, R (MU):	100	50	30	25	20	15	10	8
Average error (degrees)	1.641	1.687	2.255	2.536	2.423	4.301	6.562	7.24
Standard deviation (degrees)	1.029	1.039	1.642	1.77	1.643	3.002	4.301	4.167
Fraction of exact GBI determination (pct.)	10.5	13.0	11	11	10	8	5	6
Unsuccessful (pct.) (error > 2 pct.)	N/A	N/A	0.5	0.5	1.0	0.5	4.0	6.0

Figure Captions

Fig.1. Geometry of two Cartesian cross-sections, namely xz and yz, for a grain boundary described by $z = f(x,y)$.

Fig.2. Grain-boundary cross-sections illustrating: (a) 48 MUs (7 x 7 MU square field) neighboring the central M_0 unit and the best linear fit with its associated normal direction and (b) the situation comprising a single MU in one of the section planes.

Fig.3 Cross-sections generated using a test model to determine the accuracy of the GBI procedure: (a) Exact result for R = 50 MU and (b, c) the origin of errors for large and small grain-boundary radii, respectively.

Fig.4. Determination of the GBI: (a) Cross-section showing the grain-boundary normal estimated at point M_0 (projection within the section plane), (b) the same cross-section with several more GB normals at and near locations (indicated by the dark patches) for which the GBI procedure is not possible (c) a plot showing the fraction of grain-boundary area for which the GBI can be estimated with acceptable accuracy.

Fig.5. Dependence of effective grain-boundary mobility on misorientation angle and tilt/twist component (TTC). The bold black line corresponds to a 35° misorientation.

Fig.6. Predicted cross-sections from a 3D MC simulation of the shrinkage of an initially spherical grain (incorporating the dependence of effective grain-boundary mobility on GBI/TTC) : (a) Initial state, R = 100MU, (b) grain shape after 50 MCS, and (c) grain shape after 100MCS.

Fig.7. Initial microstructures and grain-size distributions for (a, b) Cases A and B and (c, d) Case C.

Fig. 8. MC simulation predictions of the grain-growth kinetics for Cases A, B, and C.

Fig. 9. Initial microstructure used for MC Cases D and E: (a) 3D image of selected deformed grains and some recrystallization nuclei and (b) a typical cross-section.

Fig.10. Initial stored-energy distribution (dark gray = low, light gray = high) for Cases D and E: (a) for a transverse section (b) for an in-plane section, and (c) a 3D image showing several recrystallization nuclei and the unrecrystallized volume after 50 MCS for Case D.

Fig. 11. MC predicted microstructures after 75 MCS: (a) Case D (90 pct. recrystallized) and (b) Case E (80 pct. recrystallized).

Fig. 12. Predicted recrystallization kinetics for Cases D and E.

Fig. 13. Predicted microstructures after the completion of recrystallization: (a) Case D, 100 MCS and (b) Case E, 250 MCS.

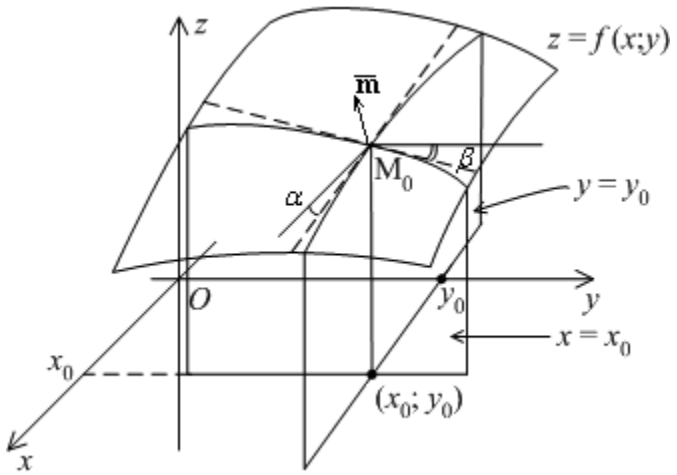

Fig.1. Geometry of two Cartesian cross-sections, namely xz and yz, for a grain boundary described by z = *f(x,y)* .

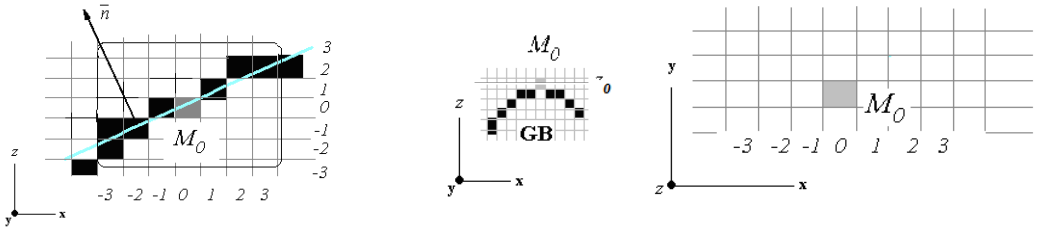

(a) (b)

Fig.2. Grain-boundary cross-sections illustrating: (a) 48 MUs (7 x 7 MU square field) neighboring the central M_0 unit and the best linear fit with its associated normal direction and (b) the situation comprising a single MU in one of the section planes.

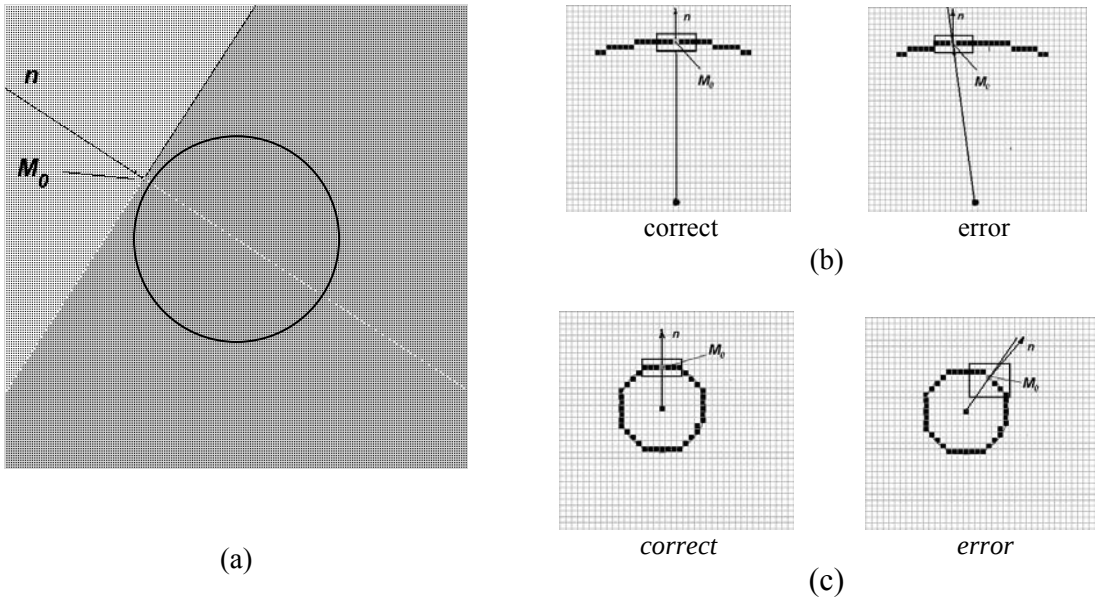

Fig.3 Cross-sections generated using a test model to determine the accuracy of the GBI procedure: (a) Exact result for R = 50 MU and (b, c) the origin of errors for large and small grain-boundary radii, respectively.

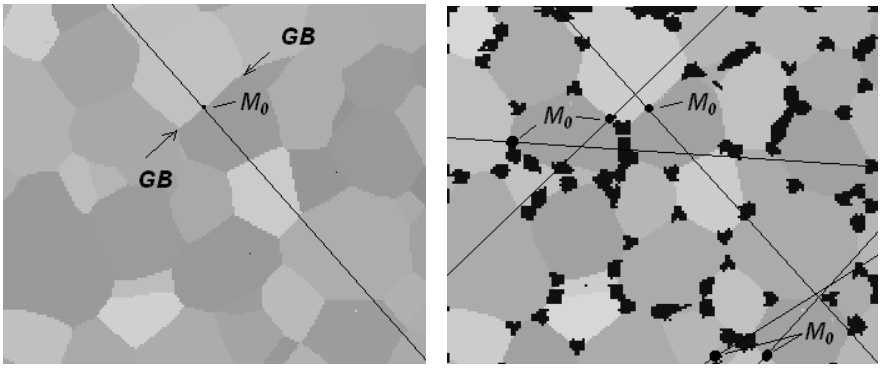

(a) (b)

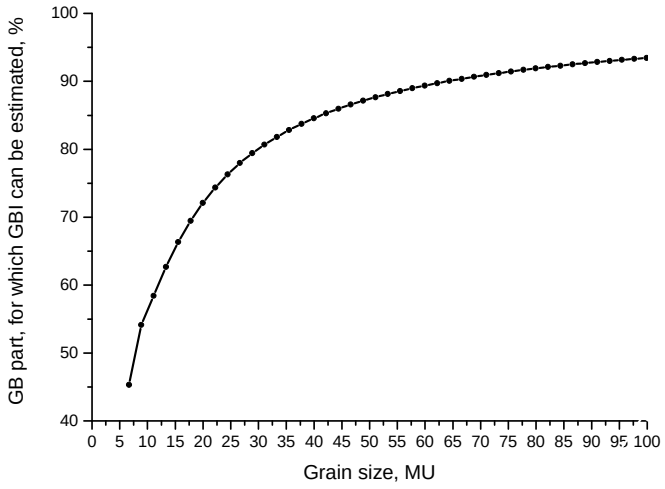

(c)

Fig.4. Determination of the GBI: (a) Cross-section showing the grain-boundary normal estimated at point M_0 (projection within the section plane), (b) the same cross-section with several more GB normals at and near locations (indicated by the dark patches) for which the GBI procedure is not possible (c) a plot showing the fraction of grain-boundary area for which the GBI can be estimated with acceptable accuracy.

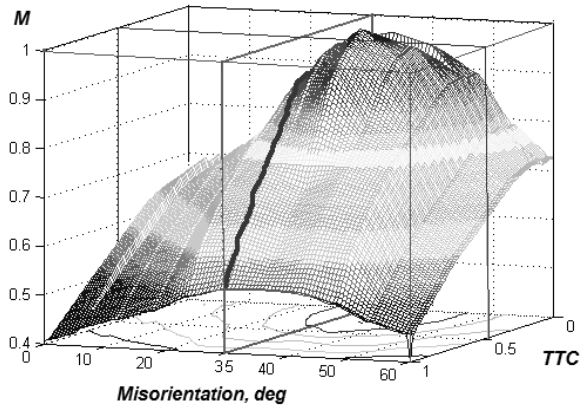

Fig.5. Dependence of effective grain-boundary mobility on misorientation angle and tilt/twist component (TTC). The bold black line corresponds to a 35° misorientation.

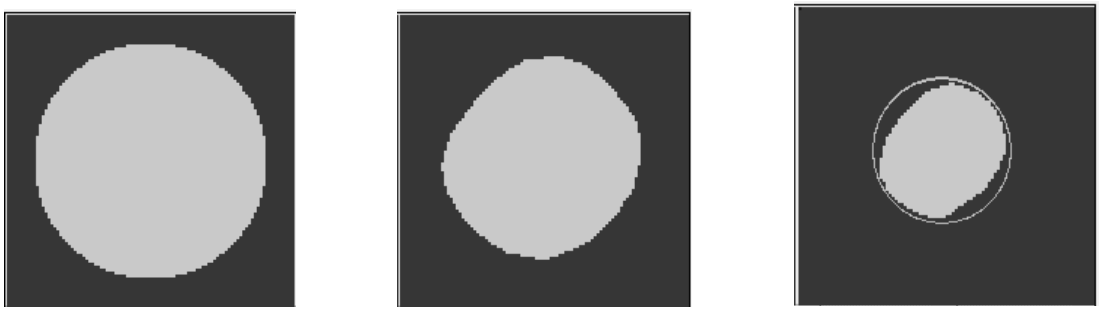

(a) (b) (c)

Fig. 6 Predicted cross-sections from a 3D MC simulation of the shrinkage of an initially spherical grain (incorporating the dependence of effective grain-boundary mobility on GBI/TTC) : (a) Initial state, R = 100MU, (b) grain shape after 50 MCS, and (c) grain shape after 100MCS.

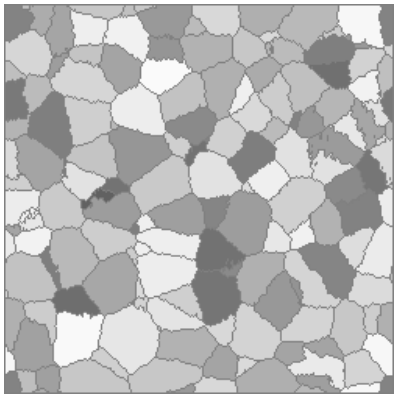

(a)

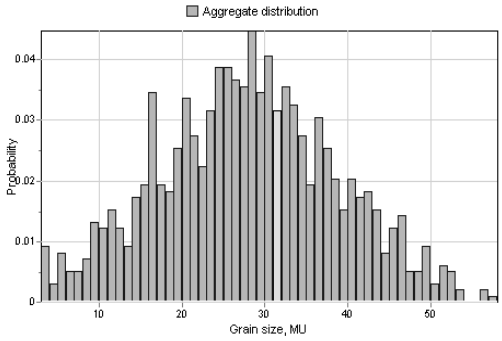

(b)

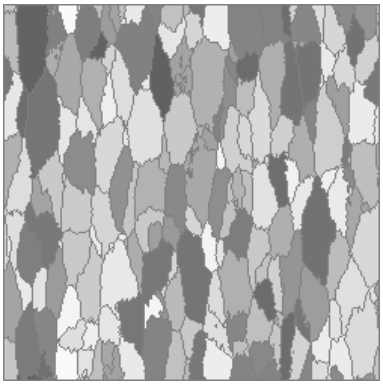

(c)

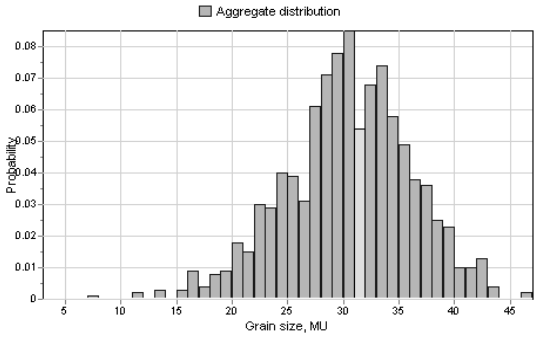

(d)

Fig.7. Initial microstructures and grain-size distributions for (a, b) Cases A and B and (c, d) Case C.

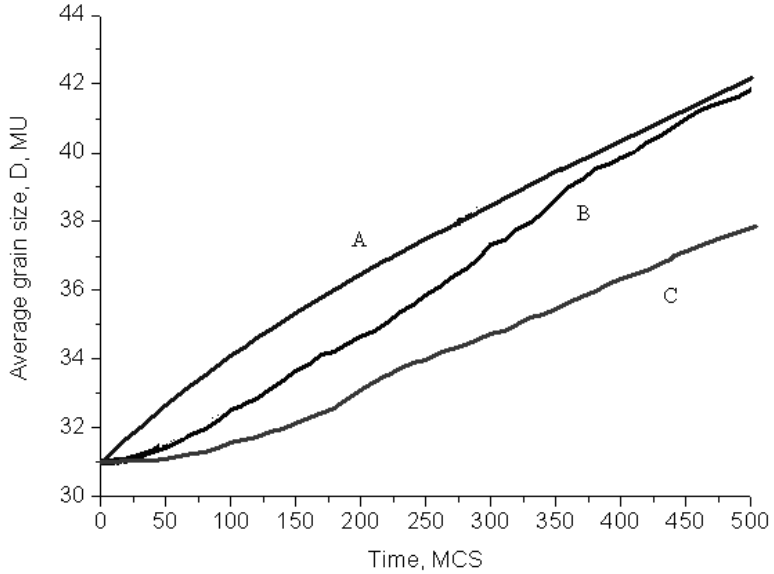

Fig. 8. MC simulation predictions of the grain-growth kinetics for Cases A, B, and C.

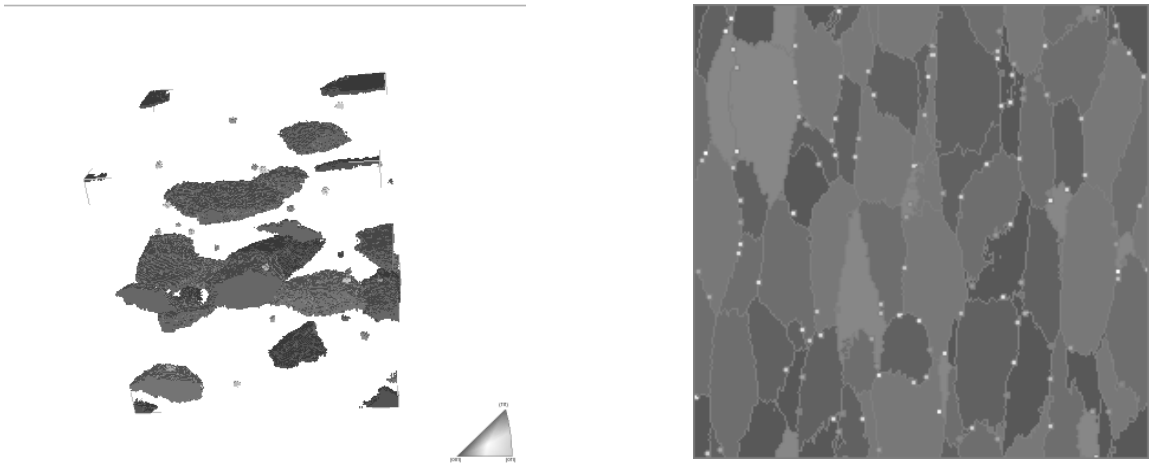

(a) (b)

Fig. 9. Initial microstructure used for MC Cases D and E: (a) 3D image of selected deformed grains and some recrystallization nuclei and (b) a typical cross-section.

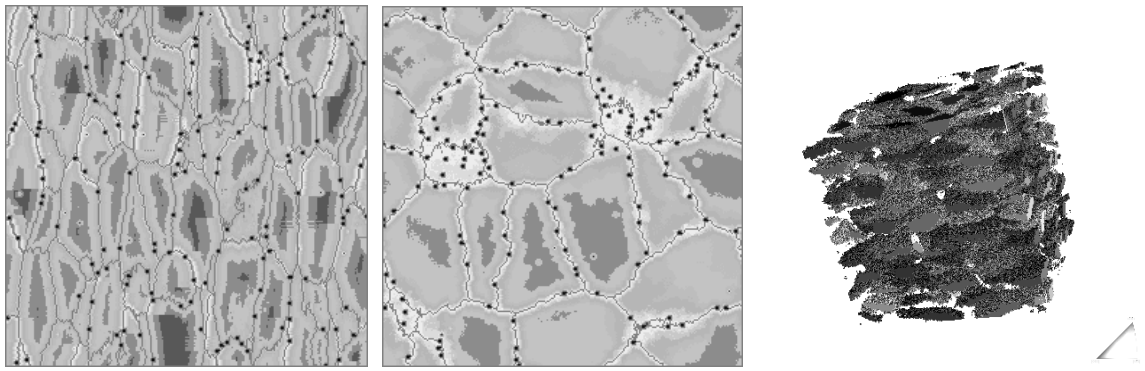

(a) (b) (c)

Fig.10. Initial stored-energy distribution (dark gray = low, light gray = high) for Cases D and E: (a) for a transverse section (b) for an in-plane section, and (c) a 3D image showing several recrystallization nuclei and the unrecrystallized volume after 50 MCS for Case D.

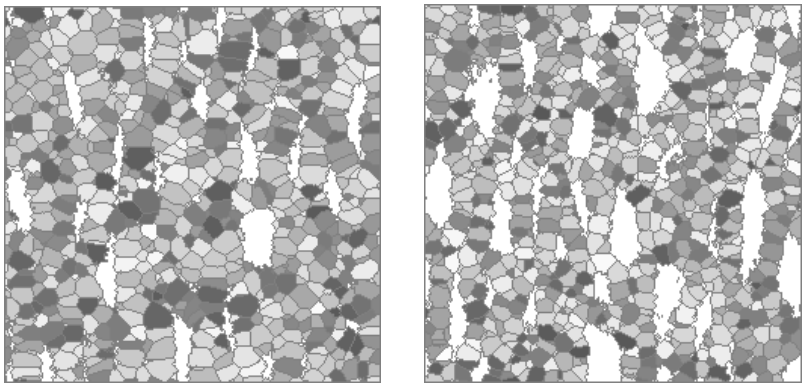

a) (b)

Fig. 11. MC predicted microstructures after 75 MCS: (a) Case D (90 pct. recrystallized) and (b) Case E (80 pct. recrystallized).

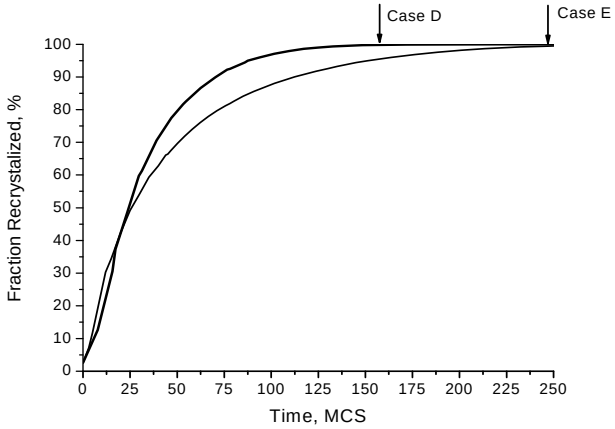

Fig. 12. Predicted recrystallization kinetics for Cases D and E.

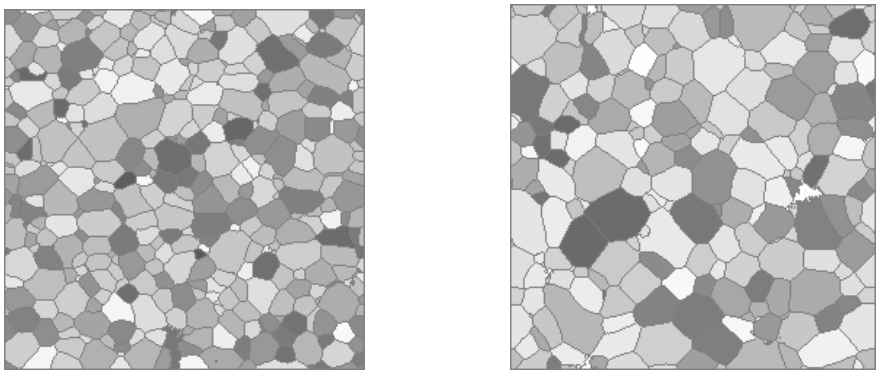

(a) (b)

Fig. 13. Predicted microstructures after the completion of recrystallization: (a) Case D, 100 MCS and (b) Case E, 250 MCS.